AIAA AVIATION Forum
12-16 June 2023, San Diego, CA and Online
AIAA AVIATION 2023 Forum

10.2514/6.2023-4428

Conceptual Design of a Strut-braced Wing Full Electric Regional Aircraft with Distributed Propulsion

Aaron Gilbrook[1]
University of Southampton, Southampton SO16 7QF, United Kingdom

Yiyuan Ma[2]
Bauhaus Luftfahrt e.V, Willy-Messerschmitt-Straße 1, 82024 Taufkirchen, Germany

and
Ali Elham[3]
University of Southampton, Southampton SO16 7QF, United Kingdom

Novel and advanced airframe and propulsion technologies serve as a priority for future aircraft design in today's climate, with the primary aim of maximising performance, and thus energy efficiency, while also exploring environmental challenges. This paper aims to incorporate novel airframe and propulsion technologies to a new fully-electric regional aircraft conceptual design, with the same top-level requirements of ATR 72-600. The aim is to design a fully battery-electric aircraft with strut-braced ultra-high aspect ratio wing equipped with distributed propulsion. The design process follows conceptual design procedures, with subsequent mission, weight and aerodynamic analysis conducted in the aircraft design environment SUAVE, modified based on the new technologies. Sensitivity analysis is also presented on the key parameters of the novel design features to greater analyse the overall effects of their implementation. The present research ultimately shows a 7% increase in energy efficiency from the ultra-high aspect ratio wing, with an additional 6% from the effects of distributed propeller propulsion.

I. Introduction

Long-term environmental goals are now at the forefront of novel aircraft design, and thus with the drive for more efficient and renewable aircraft architecture it is nonetheless essential that electric propulsion architectures are a priority for future designs. Flightpath 2050 is one such example of these goals, outlining key targets for aircraft by 2050, being a 75% reduction in CO_2 and a 90% reduction in NO_x emissions [1]. Not only does this lead to an increase in demand for fully electric aircraft, but it calls for further optimised design, particularly in performance defining areas such as the main wing of the aircraft. This work aims to define and evaluate the feasibility of a fully electric regional aircraft design for full commercial use by 2050, while also investigating the effects of novel aircraft design elements, including ultra-high aspect ratio wing design, strut bracing, as well as a fully distributed electric propellor propulsion architecture.

There are several past and ongoing projects looking into the implementation of electric propulsion into commercial aircraft; this includes both fully electric and hybridised systems. The different types of system designs can be categorised into their respective propulsive 'architectures'. Current advancements include the Boeing SUGAR Freeze, incorporating a turboelectric architecture, featuring a GE hFan+2 with electric motor [2] [3]. Examples of parallel and series hybrid electric designs include the Boeing SUGAR Volt [3] and Airbus E-Fan X [4] respectively. Research into hybrid architectures is one of the most prevalent focuses for future aircraft design, and thus it is logical that we look further

[1] Undergraduate student, University of Southampton, ajg2g20@soton.ac.uk
[2] Postdoctoral Researcher, Visionary Aircraft Concepts, Yiyuan.Ma@bauhaus-luftfahrt.net.
[3] Professor, Computational Engineering and Design Group, a.elham@soton.ac.uk

ahead to fully electric designs. One example to date using the all-electric architecture is the Ce-Liner [5]. The concept design directly relevant to this project can also be mentioned, namely the SE^2A SR developed by Karpuk et al. [6] using a battery network architecture and propellor propulsion, with performance based of an ATR-72 as the reference aircraft.

Current limitations in electrical technologies are one of the most significant challenges facing electric aircraft design. Electric motors currently do not provide sufficient power to meet the power requirements for flight. Motor resistance increases at such high power levels, thus reducing motor efficiency [3]. This results in the need for additional cooling equipment, which is detrimental through associated weight penalties [7]. High-temperature superconducting motors could be a potential solution, with theoretical power levels reaching up to 50 MW, sufficient for passenger-sized aircraft [10], and power densities in the region of 40 kW/kg, a much more promising result when compared to current motor technologies [11]. High-power, low-weight cryocooling is, however a necessary accompaniment to this, of which infrastructure does not currently exist [10]. Along with electric motor limitations is current and future battery technologies, particularly the specific energy (c_b) that they can provide. Current best case Lithium-Ion batteries produce 300 Wh/kg, which in comparison to jet fuel (1200 Wh/kg), is not nearly sufficient [7]. Thus future battery trends must be examined to select a more optimistic battery performance for use by 2050. Varied performance predictions are listed in the literature, with Lithium-Sulfur providing a supposed c_b of up to 650 Wh/kg [8], however, current demonstrated values are around 350 Wh/kg [9]. Lithium-Air batteries are suggested to have practical levels of 700 Wh/kg, and theoretical levels of 1200 Wh/kg [10]. Ultimately Lithium-Sulfur batteries offer a more refined range of theoretical values, in the region of 500 to 800 Wh/kg [8] [11] [12] [13], and thus this technology will likely be selected for the present analysis. Electric technology limitations ultimately provide a prevalent challenge for conceptual electric aircraft, and an alternative solution to combat this is the use of more efficient airframe designs.

Maximising aircraft efficiency is largely influenced by the reduction of lift-induced drag. Increasing the aspect ratio reduces this component. The adverse effect of this is significantly higher bending moments induced from the higher moment arm due to the wing loading [14]. As described by Calderon et al. [14], a method is introduced to trade off the recovered energy of increasing the aspect ratio (AR) and the additional energy required from increasing the weight using a nonlinear beam model and VLM to make drag comparisons. This, in turn, provides an optimal AR for the given design parameters. It may however be more advantageous to consider utilising a strut brace to support the additional bending moment. A proportion of the SUGAR project showed focus in comprehensively analysing this design concept [2]. The work produced in this project by NASA demonstrates strong relevance to the present research, as the research focused on high wing configurations in regional range aircraft. It is however important to consider operational limitations such as wingspan limits at commercial airports, of which mid-range passenger aircraft must conform with the ICAO Class C restriction of 36 metres. The RHEA SR-SBW concept aircraft introduced by Ma et al. [15] also analyses this concept thoroughly. Results from this study in the short-range case demonstrate a 20% reduction in fuel consumption when compared to an ATR72-600, which while not relevant to this study, is a promising result for energy efficiency nonetheless. This overall demonstrates the benefits of this concept, and it is with this research that the current project aims to further analyse its potential use in future concept aircraft.

Distributed propulsion is another feature to consider for improving the design ana, which aims to reduce noise pollution and reduce the required take-off distance for the aircraft [16]. This is achieved by spreading the propulsive power across the length of the wingspan. Other benefits which this can bring include increased engine failure redundancy, making the event of a failure far less critical [17]. As presented by Jones et al. [18], a NASA concept architecture developed for the N3-X concept aircraft features engines placed in advantageous positions along the wing such as at the wingtips to minimise the lift-induced drag as a result of wake vortices. They also place engines towards the rear of the aircraft with the aim of taking advantage of boundary layer ingestion, increasing propulsive efficiency [18].

Distributing the propulsive devices along the wing can provide an increased lift coefficient, which is particularly beneficial during the high lift phases of take-off and landing, where the highest lift at the lowest speed is desired [16]. Structural benefits to distributed propulsion are also discussed in literature, where the propulsive devices can serve to counteract lift loads in cruise, providing inertial relief, thus allowing for a lighting wing structure [19].

However, Ameyugo et al. [19] highlight limitations to distributed propulsion. The number of engines used is limited by the fact that if scaling down the engine decreases the Reynold's number such that it falls below the critical value, this can induce early separation and thus increase losses. The increasingly complex network that arises as result of increasing the number of engines will also inevitably bring associated mass penalties, as well as increased engine friction drag. Gohardani et al. [16] also make note that reducing the motor size provides a lower specific torque, and therefore a lower efficiency, particularly during cruise. A key benefit to using distributed propulsion, which serves as the main motivation for implementing this design feature into the project, is the interaction between a rotating wing-mounted propellor and the wing surface directly behind it. This is computationally researched by Aref et al. [20], who find that implementing a counterclockwise rotating propeller blade, the resulting upwash creates an increase in the local angle of attack upstream of the wing, thus increasing the local lift coefficient. This effect is also amplified by increased flow momentum [20]. Not only this, but delayed separation and stall in the wing area directly in the wake of the propellor was observed.

The aim of this paper is to provide a conceptual design of a fully electric strut-braced wing aircraft equipped with distributed propulsion. This paper incorporates a number of different design processes from literature, as well as previous work from Ma [15] and Karpuk [6], with key features of their final conceptual designs forming the basis for this present research. The ATR72-600 will provide top-level aircraft requirements for the design. We first provide the methodology we developed and used for conceptual design and then present the outcomes as well as a series of sensitivity studies.

II. Methodology for the Conceptual Design and Analysis

A. Conceptual Design Environment

The initial conceptual design is proposed as a regional sized aircraft (similar to the ATR72-600), with conventional fuselage and T-tail configurations. The main wing will feature a high aspect-ratio planform, supported by strut-bracing to alleviate the excessive loads. In combination with this, the propulsion system will incorporate all-electric technology, combined with a series of wing-mounted propellers (in the range of 8 to 12), distributed evenly along the span of the main wing.

Initial sizing has been done using the conceptual aircraft design tool developed by Ma et al. [15]. The first stage is to carry out the constraint analysis, thus determining the design point for the optimal *P/W* (power-to-weight) and *W/S* (wing loading). This is achieved through first performing an initial weight estimation to determine the total gross weight, considering the top-level requirements, as well as other mission parameters such as the payload weight. It is important to note that this estimation utilises non-conventional methodology, specifically for all-electric aircraft. As such, the required battery weight is also defined here. From this the required total propulsive power and wing planform area for the given design criteria are calculated to further define the wing parameters, provided some additional aerodynamic assumptions are used. Strut sizing can also take place here, as well as preliminary propeller sizing with the total power requirement. From here, the tail sizing can be completed, as well as some preliminary stability analysis.

An interim stage of the design process involves qualitative geometric generation within OpenVSP [21]. This is used to achieve a visual representation of the design throughout the process. It is also utilised to determine the feasibility of the propulsion architecture. More specifically, it can be used to analyse the positioning of the batteries within the aircraft. Subsequent higher fidelity analysis can then be conducted within SUAVE. The process for this involves first inputting the geometric, propulsion

and mass properties obtained during the initial sizing. The propulsion network is then incorporated in more detail, including defining the individual components and their corresponding properties, such as the motor and ESC. The ATR72-600 mission profile, including multiple climb segments, a cruise segment, multiple descent segments, as well as the addition of diversion / reserve segments, as is required for certification of the aircraft [22] is used for the design of the new aircraft. the analysis methodology of SUAVE has been modification of the structural weight calculation procedures to account for the strut-bracing, by implementing the semi-empirical methods developed by Chiozzotto [23]. The conventional propulsion weight methodology is also not sufficient, and so this has been modified to be correct for an electric transport aircraft. Besides the weight estimation, the aerodynamic analysis also incorporates the use of the wing-propeller interaction model featured in the latest version of SUAVE. The analysis is then carried out to obtained initial results for the weight breakdown, mission performance and aerodynamic performance. These values are then iterated to achieve a final design by incorporating an iteration script within the SUAVE environment to converge on the final design. The process involves a manual iteration of the required battery weight, which utilises the preliminary value determined before to determine the final required weight which achieves the full mission, with a necessary reserve factor. From this, a range of key parameters are selected such as the wing aspect ratio and the number of propellers to conduct a sensitivity analysis to determine the effect that changing these has on the aircraft performance. The overall flowchart for this design process is shown in Figure 1.

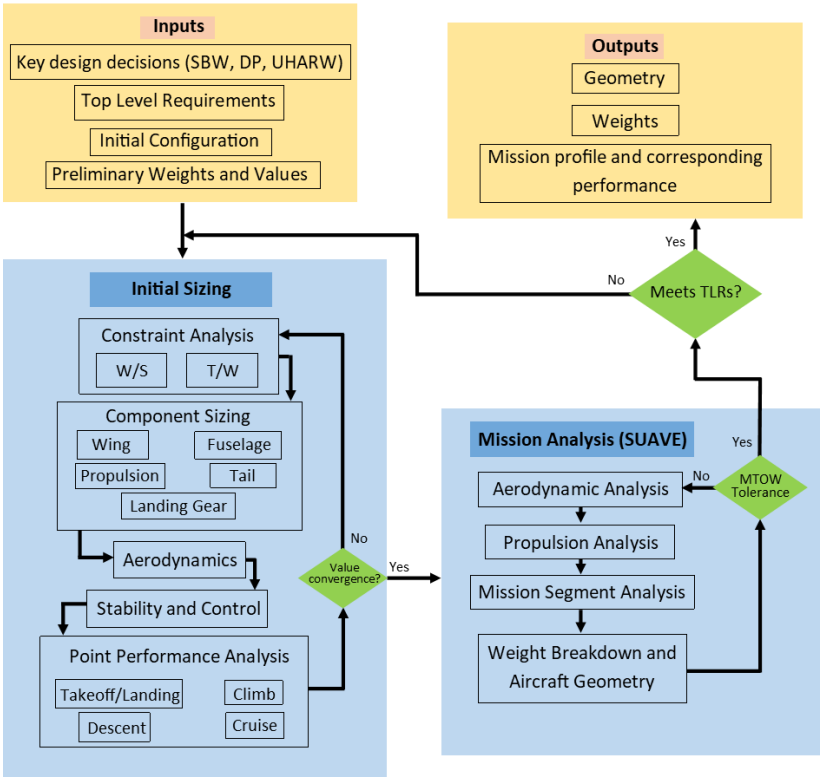

Fig. 1: Conceptual Design and Analysis Flowchart

B. Weight Estimation Method

1. Strut-braced wing weight method

Empty weight estimation of the aircraft in SUAVE takes calculations from the full range of structural components and calculates the total sum for determine the total Operational Empty Weight (OEW):

$$OEW = W_{struc} + W_{prop} + W_{sys} + W_{op} \quad (1)$$

where W_{prop} is the weight of the propulsion system, comprising of:

$$W_{prop} = w_{prop} + w_{hub} + w_{mot} + w_{bat} \quad (2)$$

where W_{sys} is the system weight, including avionics, hydraulics, electrical and control systems. W_{op} includes operational items which may be used during regular service. W_{struc} is the total structural weight:

$$W_{struc} = w_{wing} + w_{tail} + w_{fuselage} + w_{gear} \quad (3)$$

Methods for estimating the weight of these components include FLOPS [24] and Raymer [25], however for the purposes of this present analysis, an internal SUAVE method is used. The wing weight in this case must include the strut and folding mechanism contributions, and so a semi-empirical method from Ref. [23] is utilised, while the SUAVE method is retained for empennage, fuselage, landing gear and other components. The wing weight modification also considers the penalties associated with the folding mechanism, a required component of the wing design to conform to ICAO Class C restrictions on wingspan [26]. The method [23] includes separating the wing weight into its component parts:

$$m_w = k_{ail}(m_{covers} + m_{webs+ribs}) + m_{sec} + m_{strut} \quad (4)$$

where k_{ail} is the wing box mass penalty factor from aileron efficiency constraints. m_{sec} is the secondary wing weight, a function of the total gross weight. The component weights are derived as follows:

$$m_{covers} = k_e \cdot C \cdot m_{TO}^{E_e}(W/S)^{E_{ws}} AR^{E_A} \cos(\Lambda)^{E_\Lambda} (t/c)^{E_t} V^{E_V} (1+\lambda)^{E_\lambda} n_z^{E_{nz}} (1-\eta)^{E_\eta} \quad (5)$$

$$m_{webs+ribs} = k_e \cdot C \cdot m_{TO}^{E_e}(W/S)^{E_{ws}} AR^{E_A} \cos(\Lambda)^{E_\Lambda} (t/c)^{E_t} V^{E_V} (1+\lambda)^{E_\lambda} n_z^{E_{nz}} (1-\eta)^{E_\eta} \quad (6)$$

$$m_{strut} = k_e \cdot C \cdot m_{TO}^{E_e}(W/S)^{E_{ws}} AR^{E_A} \cos(\Lambda)^{E_\Lambda} (t/c)^{E_t} V^{E_V} (1+\lambda)^{E_\lambda} n_z^{E_{nz}} (1-\eta)^{E_\eta} P_{st}^{E_{pst}} \quad (7)$$

where k_e is the engine relief factor, Λ is the sweep angle at c/2, t/c is the thickness to chord ratio, V is the maximum operating speed (defined for the present design as the max cruise Mach of 0.457), λ is the wing taper ratio, η is the normalised strut attachment position, P_{st} is the strut parameter. Constants C and exponents E are different for each equation and are detailed in Ref. [23].

2. Propulsion weight method

The present design utilises propulsion weight estimations implemented in SUAVE for electric vertical takeoff and landing (eVTOL) aircraft, incorporated into the transport aircraft empty weight estimation. Propeller mass is calculated using the eVTOL method, which utilises the geometric and material properties and airfoil data to estimate the structural loads (shear / torsional) and thus the resulting mass, the flap mass based on bending, glue and paint mass, leading edge protection mass and core mass:

$$m_{prop} = m_{torsion} + m_{core} + m_{flap} + m_{shear} + m_{glue} + m_{paint} + m_{LE} \quad (8)$$

Motor weight utilises data provided by NASA for high power-to-weight motors and uses fitting techniques to size the motor according to the design torque [27].

C. Aerodynamic Analysis Method for Distributed Propellers

In order to effectively analyse the effects of the distributed propulsion architecture on the aerodynamic performance of the present design, the propeller wake model implemented in the current latest version of SUAVE can be used, which incorporates both VLM methodology (based on VORLAX [28]) when considering the aerodynamic loads on the wing, and potential flow theory (using the helical fixed wake model) to consider the resulting propeller wake and its effect on downstream lifting surfaces. The wing model utilises surfaces discretised into panels with a horseshoe vortex with trailing legs extended to infinity and a bound vortex at the quarter chord. The induced velocity is calculated at the three-quarter chord of the panel, subsequently leading to a lift and induced drag coefficient matrix, constructed over the entire wing surface [29].

For estimation of propeller performance, BEMT (blade element models) can be used, however this slipstream resolution lacks accuracy, particularly when considering interactions with lifting surfaces. As such, the HFW (helical fixed wake) model is incorporated to SUAVE (Figure 2). This model creates distributed vortex elements, representing the vorticity which is shed from the propeller blades as it rotates. The wake is calculated over a few full rotations of the propeller, such that the assumptions of momentum theory are still valid, and thus a fixed wake is reasonable for determining aerodynamic loads. Vortex strength is calculated from circulation at the blade element, which is, in turn, calculated from inflow to the propeller. A limitation of this method is that the results suffer from convergence difficulties, rather they are a balance of accuracy and computational cost. The total velocity induced by each ring of the potential of the propeller wake is calculated in a similar manner to the horseshoe vortices of the VLM method [29]. Figure 3 shows the VLM panelisation applied to the present design's lifting surfaces.

Although SUAVE provided the possibility for aerodynamic analysis of wing-propeller interaction, in this work, the OpenVSP aerodynamic model was used. This was due to current limitations of the SUAVE propeller wake model which has not yet been developed for full aircraft and mission analysis. Analysis is conducted using the propeller wake model in VSPAERO within OpenVSP, and the results are implemented into the SUAVE calculation for subsequent mission analysis with the new aerodynamic results. This involves a comparison of the lift and induced drag over the main wing surface with and without the propeller wake included in calculations. Thus, a correction factor is obtained and applied to the lift and drag coefficients within SUAVE. This of course, depends on the wing geometry and propulsor number and location, so the factor is calculated independently in each case.

This factor is then applied to the total lift coefficient and induced drag coefficient calculations of the aerodynamic analysis method within SUAVE, which is thus applied to subsequent calculations of mission performance. VSPAERO is setup using VLM aerodynamic methods for the main wing, and the propeller model is turned on and off as desired to obtain the compared results. Figure 4 demonstrates the propeller wake model and VLM methodology within VSPAERO.

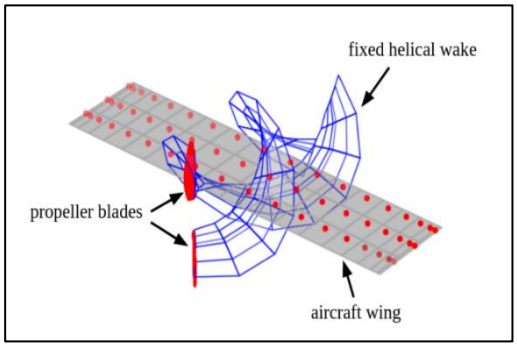

Fig. 2: Fixed helical wake model superimposed on wing [48]

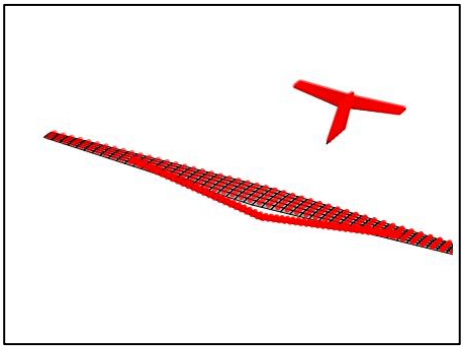

Fig. 3: SUAVE VLM panelisation of lifting surfaces

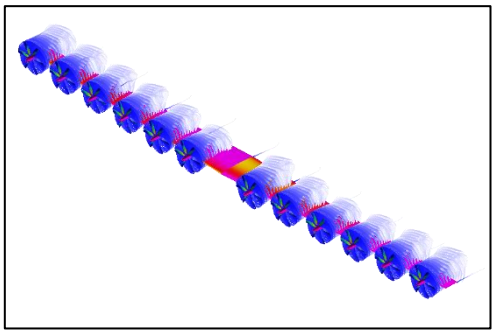

Fig. 4: VSPAERO trailing wakes and wing surface pressure

The lift and induced drag coefficients in VSPAERO are calculated with a clean wing with no propellers. The propeller model is then applied to the VSPAERO analysis with 128 wake nodes and 2 revolutions of the propellers at the desired RPM. The lift and induced drag coefficients are compared with the clean wing results to obtain the aforementioned correction factors to be applied in SUAVE.

III. Design and Analysis of a Fully Electric Regional Aircraft

In this section, a fully electric regional aircraft with strut-braced wings is conceptually designed and analyzed using the presented methods.

A. Conceptual Design

1. Initial Weight Estimation

The top-level aircraft requirements for the present design are defined referring to Refs. [30] [31], and are tabulated below:

Table 1: Top-level aircraft requirements

Parameter	Value	Units
Cruise altitude	20000	ft
Ceiling altitude	25000	ft
Enroute rate of climb	1355	ft/min
Cruise speed	270	KTAS
Max Cruise Mach	0.457	
Take-off speed	116	KTAS
Reference landing speed	113	KTAS
Landing field length	3002	ft
Range (max pax)	740	NM

The tool is then used to determine an initial total aircraft gross weight, as this serves as an input into the constraint diagrams. A simple iterative approach can be used to determine this value. Using weight estimation methodology defined by Raymer [25] for the weight fractions. This methodology was modified for electric aircraft, where the fuel weight (W_f) was replaced with the battery weight (W_b), of which is now incorporated into the empty weight (W_e).

$$W_0 = \frac{W_{crew}+W_{payload}}{1-\left(\frac{W_e}{W_0}\right)} \quad (9)$$

This requires knowledge of the weight fraction W_e/W_0, of which a reasonable value can be found from the fully electric regional aircraft battery optimised design of Karpuk et al. [6]. The payload weight is defined as 7544 kg and crew weight is 176 kg. The gross weight can then be inputted into a modified Breguet range equation [6] for electric aircraft in order to determine the required battery weight for a given range and the initial weight estimate from above.

$$R_{elec} = \frac{c_b}{g}\frac{C_L}{C_D}\frac{W_{batt}}{W_{TO}}\eta_g\eta_m\eta_p \quad (10)$$

where the corresponding efficiencies are the gearbox, motor and propeller efficiency. This also requires an initial estimate for the battery energy density. The values used are tabulated below.

Table 2: Electric aircraft range parameters

Parameter	Value	Units
Battery Energy Density c_b	700 [9]	Wh/kg
Gearbox efficiency η_g	0.95 [32]	-
Motor efficiency η_m	0.995 [33]	-
Propeller efficiency η_p	0.85 [34]	-
Lift-to-drag ratio C_L/C_D	25 [35]	-
Range	740 [30]	NM

The battery density value of 700 Wh/kg is selected as an optimistic estimate of the potential battery technology available by 2050, as established in the literature [8] [11] [12] [13]. Nonetheless it should provide a good baseline for the future use of this design. From this the battery weight is estimated, thus providing a new weight fraction for Eq. (2), and the process is iterated until convergence.

2. *Constraint Analysis*

The constraint analysis process follows methodology outlined by Gudmunsson [36]. The initial main wing aspect ratio is defined at this stage. Research carried out by Calderon et al. [18] was used to determine the initial value. The study determined the optimal value through non-linear analysis to be 19 and for linear analysis, 18. For the purposes of this design, it will be assumed that the wingspan can be maximised, with the possible addition of folding wings to overcome the limitation of wingspan limit. As such, a value of 19 was used here. This, along with top-level design requirements which have been defined above are thus entered into the equations from Gudmunsson and plotted in a constraint diagram as shown below.

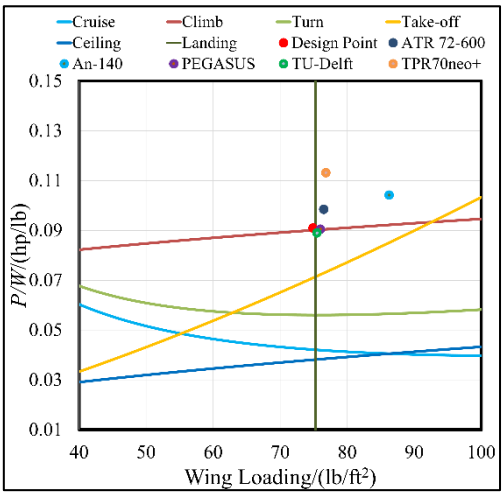

Fig. 5: Initial constraint diagram

Values for the minimum drag coefficient C_{Dmin} and the lift induced drag coefficient k, required for this constraint analysis, have been referenced from Ref. [15] for initial plots, however during aerodynamic analysis, more refined values are calculated.

The dynamic pressure is required in calculating the thrust requirements, and thus the effect of distributed propellor propulsion over the wing surface must be considered. Methodology from Patterson [37] can be used to perform analysis on a singular propellor system, thus giving an estimate for the change in dynamic pressure aft of one propellor, which can be averaged over the entire wing surface while considering the area ratio. The change in dynamic pressure over the wing surface because of the propellor slipstream is quantified using:

$$\frac{\Delta q}{q_\infty} = \frac{V_p}{V_\infty}\left(\frac{V_p}{V_\infty} + 2\right)\left(\frac{S_{blown}}{S}\right) \quad (11)$$

where V_p is the propellor slipstream velocity. This is estimated using propeller momentum theory employing the total thrust, divided by the number of propellors used to give the thrust required from one propellor system:

$$T = \rho\pi R_p^2 V_4(V_4 - V_\infty) \quad (12)$$

where R_p is approximated as the propeller radius and V_4 is the velocity far downstream; thus the effective propellor velocity V_{ep} is expressed as:

$$V_{ep} = \frac{V_4 + V_\infty}{2} \quad (13)$$

finally giving the propellor slipstream velocity as:

$$V_p = V_{ep} - V_\infty \quad (14)$$

The above methodology can thus be used to adjust the dynamic pressure in the constraint equation for the corresponding flight phase, resulting in a significant increase in wing loading at the design point, a desirable effect as the smaller wing area is optimal for reducing manufacturing costs, structural weight penalties, as well as improving the aerodynamic efficiency (L/D). This change in the overall constraint diagram can be verified using the results from Ref. [38] for a hybrid-electric distributed propulsion design, which also sees an increase in wing loading as a result of distributed propulsion.

3. Initial Parameters

The initial main wing and strut and fuselage parameters are now defined, shown in Table 3, 4, 5.

Table 3: Initial main wing parameters

Parameter	Value	Units
Wingspan b	38.7	m
Wing Area S	78.9	m^2
Taper Ratio λ	0.35	-
Sweep $c/4$	2.00	°
Aspect Ratio AR	19.00	-
Dihedral	0.00	°
Airfoil	NACA 65-618 [15]	-

Table 4: Initial strut parameters

Parameter	Value	Units
Wingspan b_{strut}	23.23	m
Wing Area S_{strut}	14.02	m^2
Taper Ratio λ_{strut}	1.00	-
Sweep $c/4$	0.00	°
Aspect Ratio AR_{strut}	38.48	-
Dihedral	11.68	°
Airfoil	NACA 65-020 [15]	-

Table 5: Initial fuselage dimensions

Parameter	Value	Units
Fuselage Length l_f	27 [15]	m
Fuselage Height w_f	2.4 [15]	m
Fuselage Width h_f	2 [15]	m

4. Propeller Sizing

Another geometric parameter defined here is the propellor diameter, which is calculated from the total required power. This can be achieved using validation from a range of methods in the literature. Kundu [39] uses an approach which defines the propeller diameter using a relationship with the installed power, using a parameter K_p, proportional to the number of blades used.

$$D_p = K_p \sqrt[4]{P} \quad (15)$$

It is noted that the diameter is limited by the tip Mach number M_{tip}, which should be kept below unity to avoid incurring aerodynamic losses [40]. Using Kundu's methodology, and using a blade number of 6, due to the use of higher blade numbers being beneficial [41], and as is used on similar regional aircraft designs [15] [6], this constitutes a K_p of 16, giving the required propellor diameter. The relationship is shown graphically in Figure 6 below.

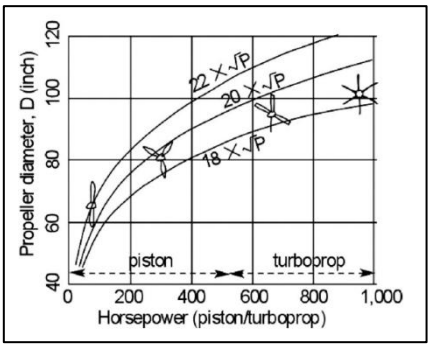

Fig. 6: Propeller diameter with increasing horsepower for varying number of blades [39]

This can also be compared to methodology from Roskam [42], who uses a blade power loading approach (Eq. 16), as well as from Howe [43], as is represented in table 6 below. The power required is determined using the P/W design point, divided by the number of engines used. This conceptual design will utilise 12 wing-mounted propellers, which conforms geometrically with the OpenVSP model.

$$P_{bl} = \frac{4P}{\pi B D_p^2} \quad (16)$$

Table 6: Comparison of different propeller sizing methods

Method	Propeller Diameter D_p	Units
Kundu [39]	1.98	m
Roskam [42]	2.11	m
Howe [43]	1.66	m

Ultimately, a propeller diameter of around 2 m is selected for the 12 identical propellers. This is sufficient to provide the required total propulsive power, although higher fidelity propeller analysis can be conducted in SUAVE utilising a wider array of parameters, including but not limited to the RPM, design lift coefficient and propeller efficiency to determine if this sizing is sufficient.

5. *Tail Configuration*

For the high wing, distributed propulsion configuration chosen here, the T-Tail was selected. Gudmunsson suggests that the use of a T-Tail invokes the horizontal tail (HT) section being placed in a flow region not in the wake of disturbed flow [36]. A conventional tail configuration with the high wing would thus lead to the HT leading edge being subjected to the main wing wake. This would subsequently reduce elevator authority due to reduced air flow over the tail surface. It must however be noted that the aforementioned advantage of the T-Tail is only true for low AoA, and that at higher angles, a phenomenon known as a deep stall may occur, which is caused by the HT being fully obstructed by the main wing wake, thus receiving no flow [44]. A trade off must be accounted for here, resulting in the T-Tail being selected as the operating conditions of the present design do not constitute prolonged periods of high AoA.

6. *Final Constraint Diagram*

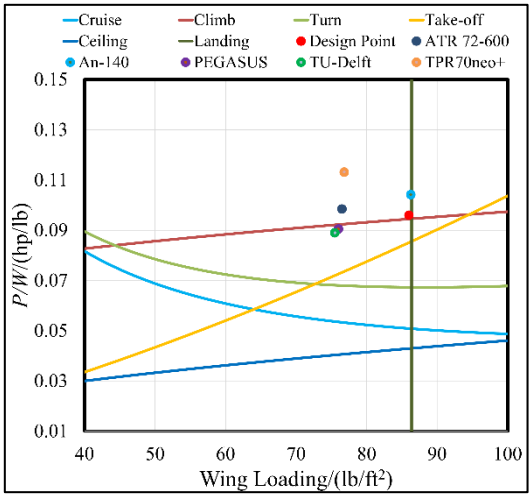

Fig. 7: Final constraint diagram

Figure 7 shows the new updated constraints as a result of the new lift induced drag coefficient k from the wing geometry and the new C_{D0} from the propeller wake disturbance. A comparison can now be made with the designs of Ma [15] and Karpuk [6]. A significantly higher wing loading is observed here, almost exclusively the result of the additional dynamic pressure. This design point positioning is heavily reliant on the landing calculation, and so this is likely an overestimate of the wing loading, which will be further analysed and iterated in SUAVE later. However, it is nonetheless evident that the additional contributions from the propeller wake across most of the wing surface are beneficial to the achievable wing loading. The power required has certainly increased compared to that of the RHEA aircraft with a similar wing aspect ratio, however the design remains feasible, and in fact offers a better power-to-weight ratio than the SE^{2}A SR design.

7. *Tail Sizing*

Tail sizing utilises a tail volume method to size the horizontal and vertical stabilizer sections according to individual tail volume ratios. After the initial tail sizing, it is important to ensure the required static margin met and the aircraft is stable for a predetermined range of aircraft CG values. Thus, a tail balance scissor plot is used within the initial sizing tool to verify that the tail size obtained from the method is adequate. After inputting the required geometric parameters and making several adjustments and iterations, a CG range of 27% is obtained, and a static margin of 14%. The final tail balance plot is shown in Figure 8, and the tail parameters are tabulated in Table 7.

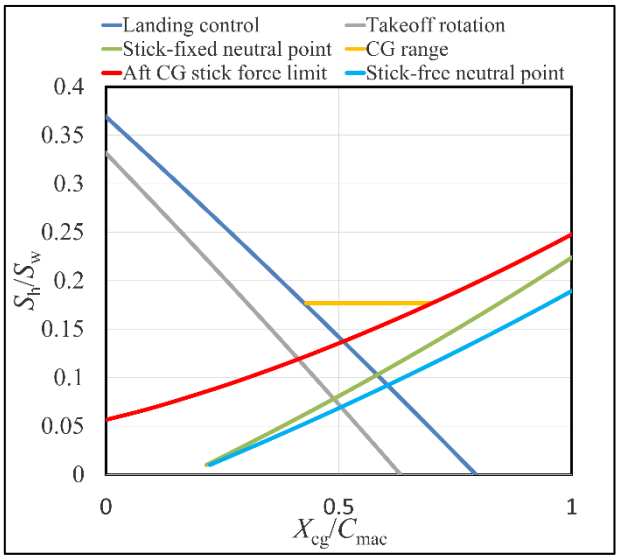

Fig. 8: Final tail balance plot

Table 7: Final tail parameters

Tail Section	Parameter	Value	Units
Horizontal Tail	Volume Ratio V_H	1.10	-
	Moment Arm L_H	13.7	m
	Aspect Ratio AR_H	5	-
	Area S_H	13.95	m^2
	Sweep $c/4$	8	°
	Taper Ratio λ_H	0.5	-
Vertical Tail	Volume Ratio V_V	0.04	-
	Moment Arm L_V	12.1	m
	Aspect Ratio AR_V	1.6	-
	Area S_V	10.1	m^2
	Sweep $c/4$	27	°
	Taper Ratio λ_V	0.67	-

8. *Final Design Parameters*

The final designed configurations' parameters are listed in Table 8 and visualized in Fig. 10.

Table 8: Initially sized aircraft final design parameters

Aircraft Subsection	Parameter	Value	Units
Weight & Power	Gross Weight W_0	33130	kg
	Battery Weight W_b	9309	kg
	Payload Weight W_p	7544	kg
	Total Power P_T	5228.7	kW
	Number of Engines n_p	12	-
	Propeller Diameter D_p	2	m
Fuselage	Length l_f	27	m
	Width w_f	2	m
	Height h_f	2.4	m
	Wetted Area S_{wf}	167.78	m^2
	Volume v_f	87.08	m^3
Main Wing (Incl. Strut)	Span b	38.7	m
	Aspect Ratio AR	19	-
	Area S	78.9	m^2
	Sweep $c/4$	2	°
	Taper Ratio λ	0.35	-
	Mean Chord c_{MAC}	2.2	m
	Main Wing Airfoil	NACA 65-618	-
	Wing Incidence θ	2	°
	Strut Attach Position	0.6b	-
	Strut Area S_{strut}	14.02	m
	Strut Taper Ratio λ_{strut}	1	-
	Strut Airfoil	NACA 65-020	-
Horizontal Tail	Aspect Ratio AR_H	5	-
	Sweep $c/4$	8	°
	Taper Ratio λ_H	0.5	-
	Volume Ratio V_H	1.10	-
	Area S_H	13.95	m^2
	Incidence θ_H	-1	°
Vertical Tail	Aspect Ratio AR_V	1.6	-
	Sweep $c/4$	27	°
	Taper Ratio λ_V	1.67	-
	Volume Ratio V_V	0.04	-
	Area S_V	10.1	m^2

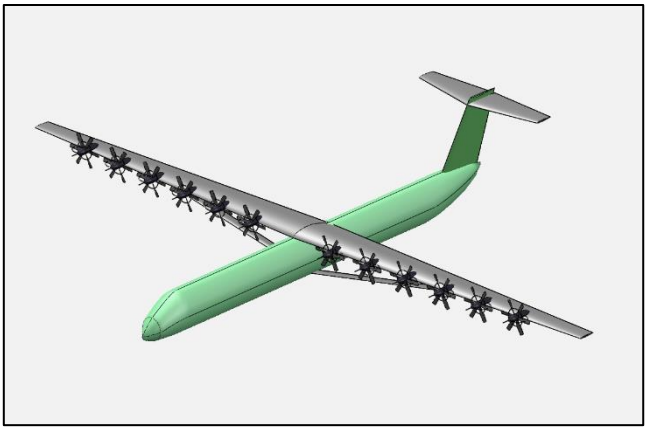

Fig. 9: Initially sized aircraft OpenVSP model

9. Battery Geometric Analysis

Prior to initialising SUAVE mission analysis, it is important to consider the implications of adding batteries to the aircraft, as the location of these will largely determine the centre of gravity positioning of the aircraft. Considerations such as how close the batteries are situated in relation to the engines, as well as the necessity for additional external geometry to accommodate the batteries is also to be considered. This first requires calculation of the total battery volume. Referring to Ref. [45], for the gravimetric energy density value chosen for this design, an ideal volumetric energy density can be expected to be in the range of 1000 Wh/L. The most logical location for the batteries would be within the main wing, and if around 50% of the volume of the main wing is usable, taking into account the internal structural components, this provides a volume of 8.99 m^3 from OpenVSP. The potential battery volume using current estimates is 6.52 m^3. Therefore, at this size, the wing volume would be sufficient to house the batteries. However, considering the distributed propulsion, and the implications this may have on the usable area within the main wing, an alternative configuration can also be considered, making use of a battery compartment underneath the fuselage. This not only allows for housing of the landing gear mechanism, but also would mean easy access to the batteries for maintenance. Utilising this configuration, a battery compartment with a wetted volume of 7.57 m^3 is chosen, giving sufficient room for the landing gear structure, as well as the entirety of the battery housing. Should the battery increase in size through further analysis, the battery compartment can either be reduced in size, or the battery volume can be shared between the main wing and the external housing.

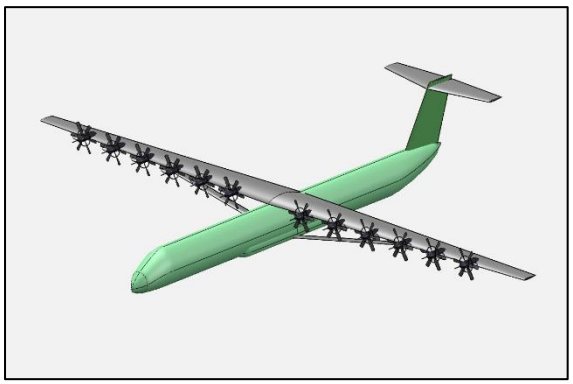

Fig. 10: OpenVSP model with battery compartment

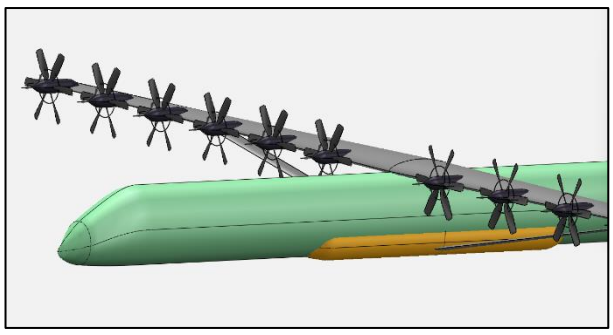

Fig. 11: OpenVSP enhanced view of battery compartment

10. *Electric Propulsion Network*

The battery propeller network implemented in the latest version of SUAVE can be used to incorporate the electric distributed propulsion architecture of the design. The proposed propulsion network is shown in Figure 12, along with the design variables inputted into SUAVE in Table 9. The propulsion architecture uses a total of 12 motors and propellers to allow for wing-mounted engine systems across the entire wing surface, with a total network voltage of 6 kV.

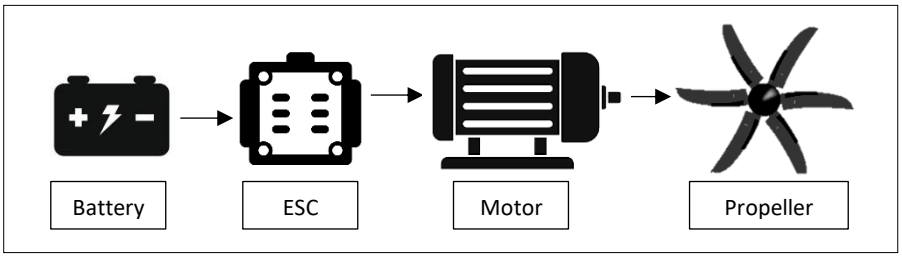

Fig. 12: Propulsion network diagram

Table 9: Propulsion network parameters

Component	Parameter	Value	Units
Battery	Total Weight W_b	9309.3	kg
	Specific Energy c_b	700	Wh/kg
	Resistance R_b	0.005	Ohms
	Max Voltage V_b	6000	V
ESC	Efficiency η_{ESC}	0.98	-
Motor	Nominal Voltage V_m	2250	V
	No Load Current A_m	0.05	A
	Efficiency η_m	0.995	-
Propeller	Number of Blades B	6	-
	Angular Velocity Ω	5000 [46]	RPM
	Tip Radius $R_{p,tip}$	1.175	m
	Hub Radius $R_{p,hub}$	0.2	m
	Design Power P	435.7	kW
	Design Lift C_{Lp}	0.8	-

11. *Mission Profile*

The mission profile, including a main mission and a reserve segment, is inputted into SUAVE utilising the initial top-level parameters as a baseline. These support in defining the cruise altitude, cruise speed, climb rate and total design range. Using these parameters, the mission profile utilised for analysis is shown graphically in Figure 13.

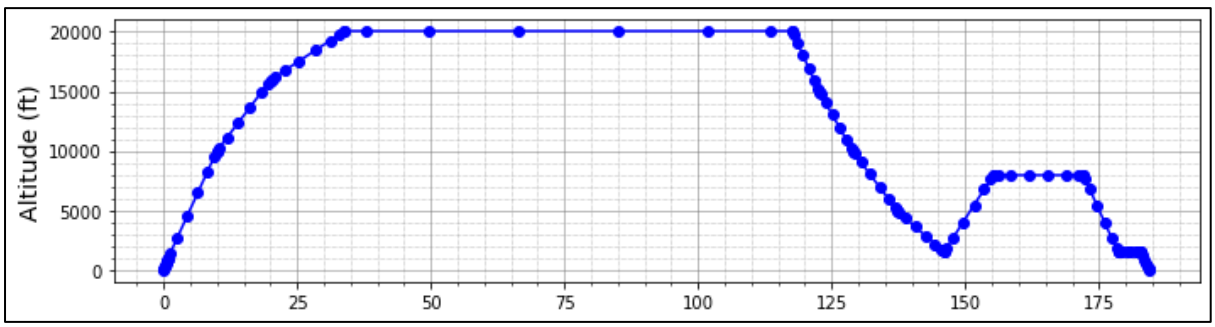

Fig. 13: Design mission profile

B. Performance Analysis

The initially sized aircraft is imported into the SUAVE environment, and the analysis is carried out using an iterative approach. The wing loading constraint determined during initial sizing is used as the criteria for SUAVE iteration to produce fully converged results. This is achieved through using the outputted weight breakdown of the previous iteration to update the area of the lifting surfaces accordingly. A manual iteration of the battery weight was conducted to achieve a 5% margin of battery energy available upon completion of the mission. This 5% margin is utilised as a final reserve safety factor. Updated aircraft geometry is thus outputted from this, as well as a final comprehensive weight breakdown table and aerodynamic performance results through the VLM calculations. The design analysis is conducted with and without the wing-propeller correction for comparison, and the following data is converged after 6 iterations of the SUAVE procedure.

Table 10: Iterated aircraft geometric parameters

Group	Parameter	Iterated Design	Iterated Design (with wing-propeller correction factors)	SE^{2}A SR	RHEA SR-SBW	ATR72-600	Units
	S_w	80	77.8	136.0	60.9	-	m^2
Main Wing	b	38.9	38.4	38.7	39	27.1	m
	c_r	3	2.9	4.68	2.3	-	m
	c_t	1.1	1.0	-	0.8	-	m
	λ	0.35	0.35	0.5	0.35	-	-
	AR	19	19	11.0	25	-	-
	S_H	14.3	13.6	-	11.8	-	m^2
Tail	b_H	8.4	8.3	-	7.7	-	m
	AR_H	5	5	-	5	-	-
	λ_H	0.5	0.5	-	0.45	-	-

Table 10 shows the updated wing and horizontal stabiliser. These results highlight the benefits that the additional lift factor brings to the present design when considering the wing-propeller interaction effect. The iterated design without wing-propeller correction shows an increase in all key wing and horizontal stabiliser parameters. This is the result of an increase in the weight breakdown when compared to the initially sized aircraft. This, when iterated to enforce the constant wing loading, leads to an increase in wing and thus tail area. With the wing-propeller model incorporated, the design instead shows a decrease in wing and tail sizing, as a result of the lower battery weight, thus demonstrating more efficient aircraft geometry from improved aerodynamic performance. This consolidates promise for the distributed propulsion architecture. The dimensions of the SE^{2}A SR electric aircraft are shown here for reference, and the key differences to note are the reduced wing area and chord from the higher aspect ratio. A reduction of 4% wing area can be observed for the iterated design, and a 4.2% reduction with propeller wake contributions. The main wing and horizontal stabiliser dimensions are much comparable to the RHEA SR-SBW aircraft, the noticeable difference being the higher main wing AR, and thus even further reduced wing area compared to the SE^{2}A SR aircraft. Nonetheless, the wing area of the present design is much closer to that of the RHEA aircraft.

Table 11: Iterated aircraft weight breakdown

Group	Subsection	Iterated Design	Iterated Design (with wing-propeller correction factors)	SE^{2}A SR	RHEA SR-SBW	ATR72-600	Units
	W_0	33611	32651	35369	22229	22800	
Total Weights	W_e	24940	23980	27869	12821	13500	
	W_{oe}	26263	25303	-	-	-	
	W_{fuel}	-	-	-	1432	2000	
Structural Weight	*Wing*	2609	2521	-	2103	-	
	Tail	574	558	-	513	-	
	Fuselage	2193	2196	-	2497	-	
	Landing Gear	1344	1306	-	643	-	
	Total	6720	6582	-	5756	-	kg
Propulsion Weight	Propellers	329	322	-	-	-	
	Motors	530	530	-	-	-	
	Total (incl Avionics)	874	867	-	1019	-	
System Weight	Systems	5427	5409	-	-	-	
	Battery	11919	11122	12783	-	-	
	Total	17346	16531	-	5579	-	

The weight data in Table 11 shows the additional gross weight implications of using electric propulsion as opposed to the conventional fuel systems of the RHEA SR-SBW and ATR72-600. This additional weight is imposed on the structure (wing and landing gear), as well as the much heavier energy storage solution. A point to note is the lower propulsion weight compared to the twin-engine RHEA aircraft, where one might expect the utilisation of more propellers to impose a higher weight. This is perhaps the result of a difference in weight estimation methods; however, the results are nonetheless promising from the standpoint of feasibility, in that there no associated inhibiting weight penalties.

Table 11 presents the same trends shown in the geometric parameters. The reduction in wing and tail areas from the propeller wake model leads to an overall reduction in structural weight. The propeller weight is also reduced through lower power requirements, and the systems weight also sees a reduction. From a performance perspective, this initial analysis suggests that the ultra-high aspect ratio wing does indeed constitute a lower battery weight from reduced energy consumption. The structural penalties of the more complex wing structure through strut-bracing do not outweigh the gains in aerodynamic performance. The initial weights (without wing-propeller model) demonstrate a 7% reduction in energy consumption compared to the SE^{2}A SR as a direct result of the ultra-high AR strut-braced wing. This result is comparable to the higher fuel efficiency of the RHEA SR-SBW over the ATR72-600. It is interesting to note that the performance gains are less significant for the electric aircraft designs, compared to the 28% fuel efficiency increase of the RHEA aircraft. The wing-propeller interaction benefits offer a further 6% improvement in energy efficiency over the SE^{2}A SR, suggesting even greater performance benefits from not only the aerodynamic improvements but also the geometric and thus structural reductions as a result. The incorporation of both novel technologies, when directly compared to the battery weight of the SE^{2}A SR, ultimately suggest up to 13% improvement in energy efficiency, and thus the same mission requirements can be achieved with lower structural, propulsion, and system weight, offering a more competitive design.

Table 12: Aircraft aerodynamic results

Parameter	Present Design	Present Design (with wing-propeller correction factors)	RHEA
C_L	0.65226	0.65306	0.685
C_D	0.03436	0.03345	0.029
L/D	18.98	19.52	23.59

Table 12 presents a comparison of aerodynamic results. A reduction in drag is observed from the wing-propeller model, an unexpected result due to the direct proportionality of lift to induced drag. The results here are from the cruise phase of the mission analysis, and SUAVE is constructed such that additional lift results in reduced pitch to maintain constant C_L. This therefore constitutes a reduction in drag. Thus, the L/D is the better result to compare here. The high performance of the RHEA aircraft appears to be reduced for the present design, despite similar airframe technologies. This is likely the result of the increased gross weight of the electric aircraft, and thus increased drag, additionally from the more complex propulsion system. The RHEA aircraft also features a higher AR. Nonetheless, the wing-propeller model does indeed constitute an increase in the L/D (around 3%), which agrees with the improved energy efficiency. Ultimately, although the L/D is higher when compared to conventional aircraft of the same design range, the results are not as significant as that of the RHEA aircraft. This explains the less significant increase in energy efficiency as a direct result of the ultra-high AR wing between the SE^{2}A SR and the present design (7%), and the RHEA-SR SBW and the ATR72-600 (28%). Figures 14 and 15 show the overall mission performance results for the present design outputted from the SUAVE analysis.

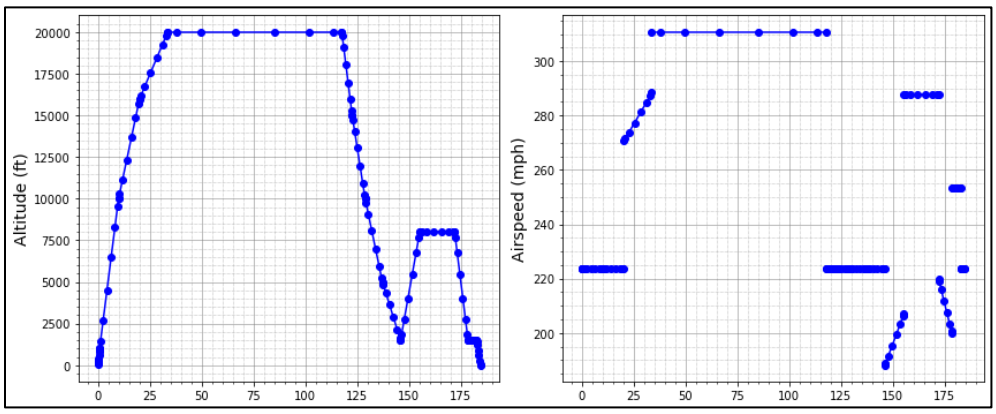

Fig. 14: Overall mission performance results

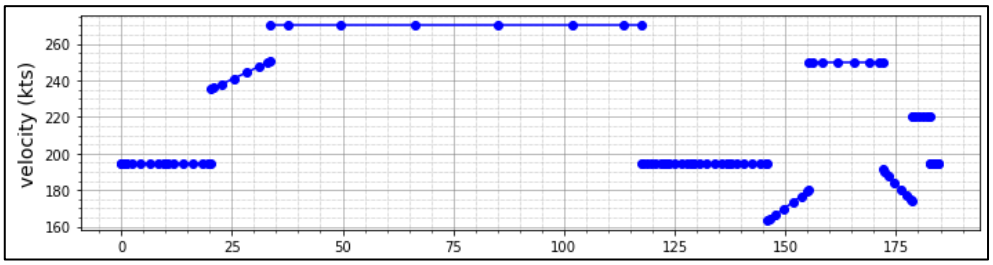

Fig. 15a: Mission velocity results

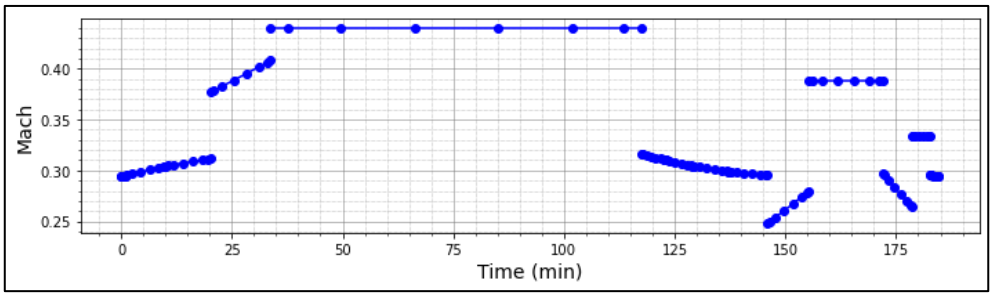

Fig. 15b: Mission Mach results

A comparative analysis of the results with and without and the wing-propeller model can also be carried out.. The results show the improvements to L/D in cruise phase (around 3%), as previously compared, however these plots also highlight that the most significant gains of the distributed propulsion are seen during climb and descent, where the L/D is increased by over 18% at its peak. As such, energy efficiency improvements are likely to be mostly gained during the climb and descent phases of the mission, where high lift is more essential, and thus has a greater bearing on the aircraft performance. The climb and descent L/D is within a more comparable range to that of the RHEA SR-SBW aircraft performance and demonstrates that despite the much higher gross weight of the electric aircraft, the design is still capable of achieving high aerodynamic performance with the aid of distributed propulsion.

Battery energy results show further demonstrate the improvements to energy usage over the course of the selected mission. This is evident through the clear lower rate of battery discharge when the distributed propulsion effects are applied. To quantify the greater performance gains of the climb phase compared to cruise, a 9.9% improvement in energy efficiency is seen for the climb phase, compared to a 6% improvement over cruise. This calls into question the need for a more comprehensive comparative study of independent mission phases, as the performance improvements have a clear dependence on the mission parameters for which the aircraft is being analysed for. Thrust results can also be compared, and results show a reduction in thrust requirements. More noticeable improvements are once again shown to be during the climb and descent phases, where the additional lift constitutes less thrust to achieve the same vertical speed. Thrust requirements are reduced by 5% for the climb phase, compared to 2% for the cruise phase. It remains important to note however, that this comparison is made between results for the same aircraft design, and thus the performance benefits cannot be said to also be true when compared to conventional propeller propulsion, namely the twin-engine architecture. Therefore, sensitivity analysis of the number of propulsors is needed to further develop understanding and perspective on the true improvements that can be gained from this technology. Figure 16 shows the present design model in OpenVSP after the full SUAVE iterative procedure for reference.

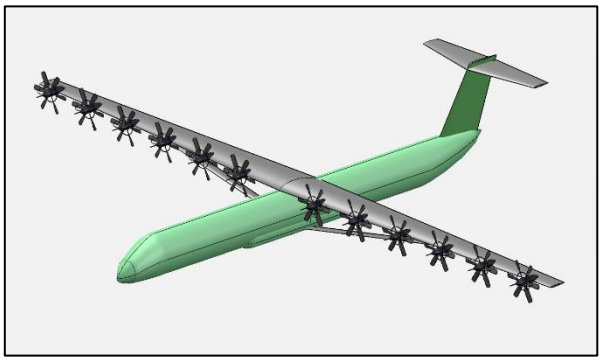

Fig. 16: Final OpenVSP model of aircraft design

C. Design Space Exploration

In this section, sensitivity analysis is conducted for the wing aspect ratio, propulsor number, and specific battery density to explore the potential performance of the full electric regional aircraft.

1. Aspect Ratio Sensitivity Analysis

The wing AR can now be varied to perform a sensitivity analysis on the total aircraft performance, measured by the battery weight in each case. The analysis is carried out for a constant wing area. The wing-propeller model is not used for this analysis for faster computing time, and the results should regardless be independent of this factor.

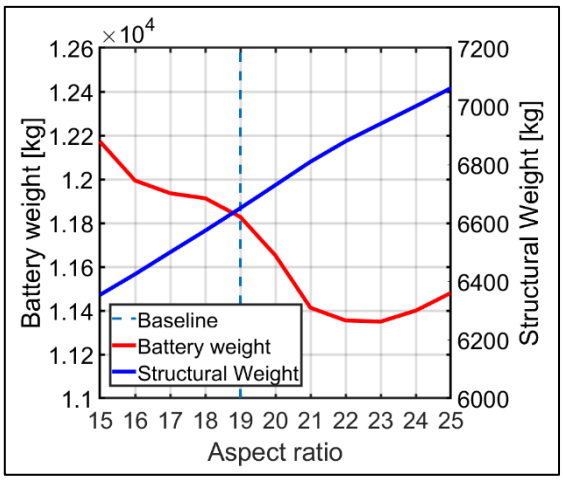

Fig. 17: Aspect ratio sensitivity analysis

This analysis (shown in Figure 17) demonstrates the bearing in which the wing AR has on the aircraft performance. Increasing the aspect ratio between 15 and 21 coincides with decreasing battery weight, before levelling off and eventually beginning to increase. What differs here is the slowing rate of decline in battery weight, particularly around 17 and 18. The reasoning behind this aspect of the results is unclear, however wider analysis of the entire range of ARs suggest a clear decline in energy efficiency at this particular wing geometry.

Table 13: Aspect ratio sensitivity aerodynamic results

AR	15	16	18	19	20	21	25
L/D	18.49	18.75	18.79	18.99	19.19	19.63	19.38

The L/D results displayed in Table 13 show clear correlation to the corresponding battery weight results. This result suggests that the wing geometry has decreased efficiency benefits for ARs between 16 and 18, while higher AR results suggest that the current aircraft design can be further optimised. However, the AR can only be increased to around 22, at which point the performance benefits are diminished, and further increase results in weight penalties. This trend can be explained by the increase in structural weight. This is a result of the increased wingspan, thus calling for greater structural penalties, which are not sufficiently high for ARs up to around 23, but beyond this the weight penalty becomes detrimental to aerodynamic performance and ultimately energy efficiency. Comparing with the RHEA results for aspect ratio sensitivity, this limit occurs at a lower AR than that of Ma's design (around 26 [47]), and thus suggests that the performance benefits are more limited for this fully electric

aircraft compared to conventional propulsion. This of course coincides with the limited efficiency gains mentioned previously when comparing the gains over the SE^2A SR (7%) with the RHEA's gains over the ATR (28%). This ultimately highlights room for further performance improvements for the present design, of which an increase in aspect ratio would prove beneficial to a certain extent, with battery weight reductions as much as 4% here, but also highlights that the potential performance is limited when compared to the conventional propulsion design of the RHEA aircraft.

2. Number of Propulsors Sensitivity Analysis

The sensitivity analysis can be extended further to better quantify the performance enhancements of distributed propeller propulsion, compared to conventional twin-engine propulsion. Prior aerodynamic analysis was carried out in OpenVSP for a range of propeller configurations (2, 4, 6, 8, 10, 12), of which the propeller position and diameter was adjusted accordingly, and unique correction factors were obtained in each case. Figures 18a to 18d show the difference in the model for different configurations in OpenVSP, and Figures 19a to 19d show the outputted trailing wakes from the VSPAERO analysis with the propeller interaction model active.

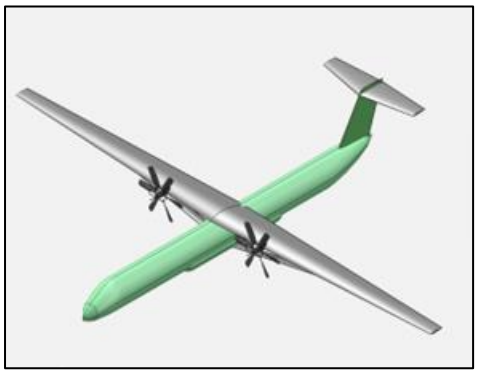

Fig. 18a: OpenVSP model for 2-propeller configuration

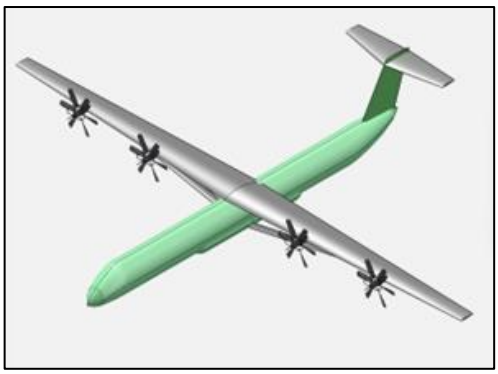

Fig. 18b: OpenVSP model for 4-propeller configuration

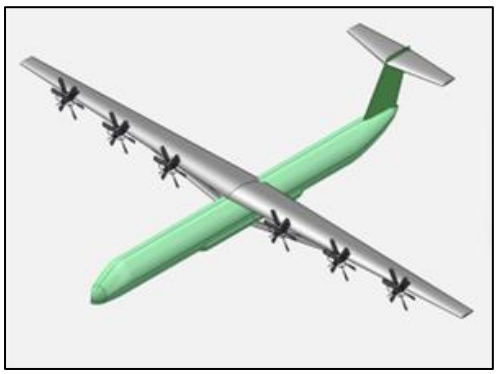

Fig. 18c: OpenVSP model for 6-propeller configuration

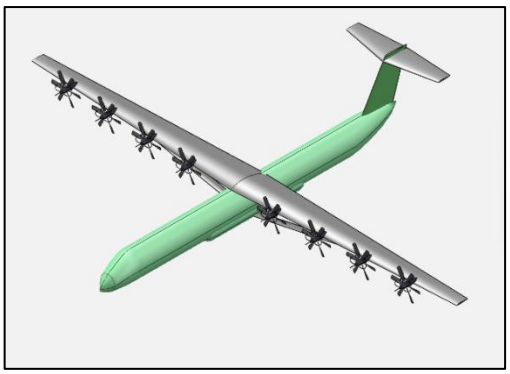

Fig. 18d: OpenVSP model for 8-propeller configuration

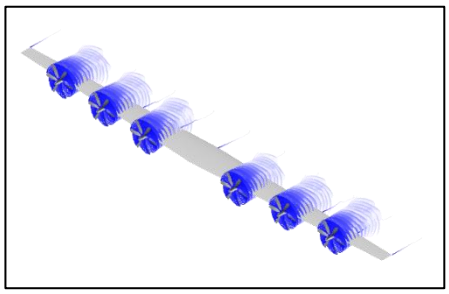

Fig. 19a: VSPAERO trailing wakes for 6-propeller configuration

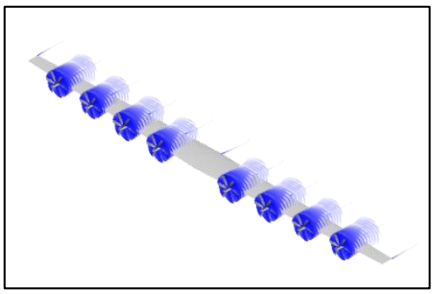

Fig. 19b: VSPAERO trailing wakes for 8-propeller configuration

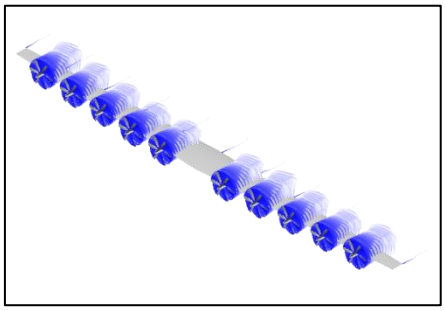

Fig. 19c: VSPAERO trailing wakes for 10-propeller configuration

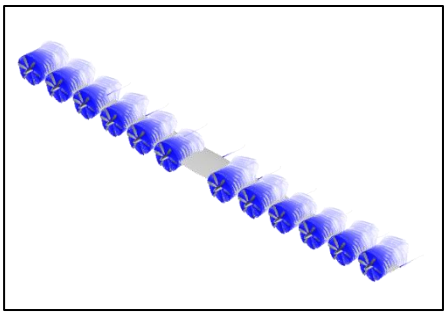

Fig. 19d: VSPAERO trailing wakes for 12-propeller configuration

After the corresponding correction factors, propeller diameter and positions are obtained, the new model is applied to the SUAVE analysis, and the results are compared through the range of configurations. The RPM in each case is also adjusted to match the new propeller diameter, which is tabulated in Table 14 alongside the aerodynamic results for reference.

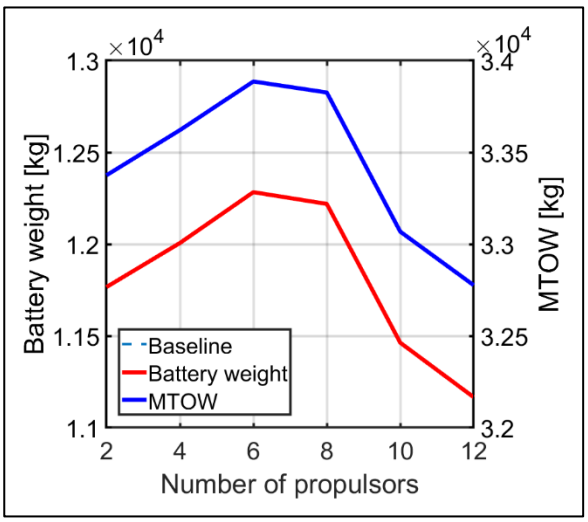

Fig. 20: Number of propulsors sensitivity analysis

Table 14: Number of propellers sensitivity aerodynamic results

Number of Propellers	2	4	6	8	10	12
L/D	19.05	19.14	19.23	19.34	19.44	19.52
RPM	2500	3000	3500	4000	4500	5000

The battery weight data in Figure 20 shows an increase as the propeller number is decreased from 12, and shows that utilising 6 to 8 propellers is in fact more detrimental to the energy efficiency. Results show improvement at lower propeller numbers (2 to 4) as the propulsive efficiency will increase with increasing propeller diameter [25]. The results present the idea that while increasing from 2 propellers to 4, 6, or 8 propellers shows damaging performance results, further increasing the propeller number beyond this does in fact show to eventually improve the energy efficiency. Ultimately, the increase in lift contributions is much higher for the higher propeller number (10 to 12), and as such the decline in propulsive efficiency is overtaken by the aerodynamic performance.

The present analysis methodology involved utilising C_L and C_D results from an independent environment, and the results within VSPAERO may not coincide fully with SUAVE. VSPAERO results for lift and drag ultimately appear to lack accuracy and therefore it must be said that this analysis is only presented to highlight any obvious trends. Quantifying the magnitude of performance increase or decrease here would be inappropriate, and as such this research requires further analysis to more definitively prove or disprove the benefits of distributed propeller propulsion. A conclusion that can however be made from the results above is that while the higher propeller number of 12 used does show definite potential for improving the performance of aircraft of this scale, it remains to be said as to whether this architecture can truly provide better performance over conventional propeller architectures.

3. Battery Density Sensitivity Analysis

It is crucial to analyse the sensitivity of the present design to future battery technology availability to fully determine the feasibility of this design for real-world use by 2050. The current design procedure has used a constant value of 700 Wh/kg for the battery pack energy density, as was estimated from the relevant literature. There is no doubt uncertainty to this value, and the extent to which changes in this affect the design must be considered. With this, the energy density can be varied from 500 Wh/kg to 1000 Wh/kg to scrutinise the performance impacts, and ultimately the significance of this design parameter to the overall aircraft performance, quantified once again by the total battery weight. The baseline design point at 700 Wh/kg is of course included.

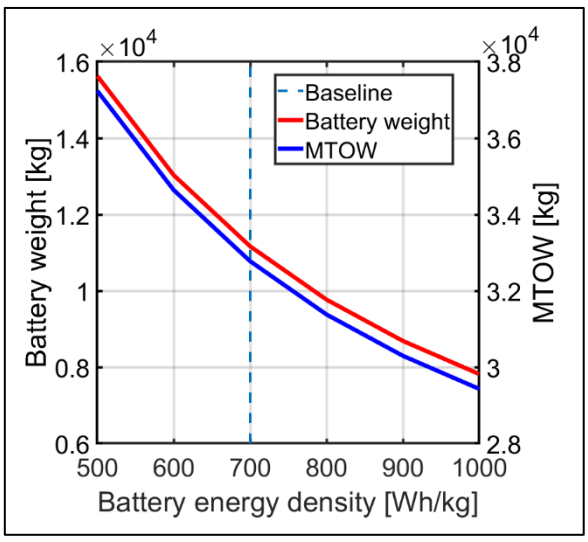

Fig. 21: Battery density sensitivity analysis

The trend observed in Figure 21 for varying battery energy density shows that the present design is more sensitive to decreases in this value, than increases. The trend shows that as battery energy density is increased, the corresponding battery weight reduction decreases in magnitude. As such, the performance results obtained for the present design are heavily reliant on battery technology trends reaching the value specified of 700 Wh/kg at a minimum, with further increases showing increasingly

smaller, but nonetheless still significant improvements in energy efficiency. As there is a sizable amount of uncertainty around this parameter, and the value chosen is based off future projection metrics and estimations from literature, the design remains dependent on technology following closely to these predictions. It therefore leaves a prominent question as to the design's realistic feasibility, but nonetheless the analysis still serves the purpose of presenting a numerically competitive design within the technology metrics in which the designs of Ma [15] and Karpuk [6] also reside in.

IV. Conclusions

The current research has presented a full design procedure and final conceptual regional commercial aircraft design candidate which aims to achieve future performance goals within aviation by 2050, with the priority being to minimise emissions and achieve maximum energy efficiency. This was achieved through comprehensive geometric and gravimetric initial sizing, followed by higher fidelity mission, weight and aerodynamic analysis. The paper introduced a combination of novel technologies, including an ultra-high aspect ratio strut-braced wing, fully electric propulsion architecture and distributed propeller propulsion, combined in unison with the hopes of offering better performance to the conventional designs. This was ultimately quantified through comparison of the total required battery weight, and thus the amount of energy required to achieve the design mission requirements.

The analysis conducted in the presented conceptual design and analysis method displayed promising results for the technologies used. A comparison with the battery weight of the reference aircraft showed 7% increase in energy efficiency, and thus reduction in battery weight, as a direct result of implementing a high aspect ratio strut-braced wing. The additional weight contributions of the wider wing structure and supporting strut did not outweigh the additional L/D achieved with this configuration. Comparison of the present design with and without the additional lift and drag contributions from the wing-propeller interaction model showed that the distributed propulsion has the potential to offer at least 6% in additional energy efficiency, directly achieved by further increasing the L/D achieved by the aircraft, and so with further analysis, the combination of the two technologies does show some initial promise to offering a competitive fully electric regional aircraft.

Further investigation through iterative design and subsequent full mission analysis revealed that the reduction in battery weight as a result of the incorporated technologies results in reductions to structural, propulsive and system weights and thus provides a more efficient and cost-effective design candidate. Continued comparative analysis of the wing-propeller model demonstrated that the most considerable benefits arose during the climb and descent phases of the design mission, with up to 18% additional L/D in climb, compared with 3% in cruise. This ultimately leads to significant energy efficiency improvements across these stages of the mission, with a reduction in thrust also noted to be more significant during climb and descent, compared to cruise.

Subsequent sensitivity analysis, while bringing forth some interesting trends for the aircraft performance, ultimately generated some potential limitations for the particular technologies used. Analysis of the aspect ratio sensitivity, while showing room for further performance benefits, ultimately showed limitations for higher aspect ratios (beyond 23) where the additional structural weight penalties overtake any aerodynamic improvements. Battery energy density sensitivity analysis demonstrated the reliance of the design on future battery technology reaching at least the value specified by 2050, and that should technology not reach this point, the performance results will be greatly diminished. Lastly, analysis of the number of propulsors certainly proved that the higher number of propulsors (12) does offer additional energy efficiency over a smaller number (6 to 8) with increased L/D benefits, but it also brings light to the reduction in relative performance when comparing a propulsion architecture of 2 to 4 engines, where the propulsive efficiency improvements of the larger propeller diameter ultimately prevail. Thus the question remains as to the true performance gains that this particular architecture offers over conventional propulsion configurations.

V. References

[1] A. Krein and G. Williams, "Flightpath 2050: Europe's Vision for Aeronautics," *Innovations for Sustainable Aviation in a Global Environment,* pp. 63-66, 2012.

[2] M. K. Bradley and C. K. Droney, "Subsonic Ultra Green Aircraft Research: Phase II – Volume I – Hybrid Electric Design Exploration," NASA/CR–2015-218704/Volume I, 2015.

[3] P. Wheeler, T. S. Sirimanna, S. Bozhko and K. S. Haran, "Electric/Hybrid-Electric Aircraft Propulsion Systems," *Proceedings of the IEEE,* vol. 109, no. 6, pp. 1115-1127, 2021.

[4] D. B. Jayme, "Evaluation of the Hybrid-Electric Aircraft Project Airbus E-Fan X," HAW Hamburg, Hamburg, 2019.

[5] M. Hornung, A. T. Isikveren, M. Cole and A. Sizmann, "Ce-Liner - Case Study for eMobility in Air Transportation," in *2013 Aviation Technology, Integration, and Operations Conference, Los Angeles CA*, Munich, 2013.

[6] S. Karpuk and A. Elham, "Influence of Novel Airframe Technologies on the Feasibility of Fully-Electric Regional Aviation," *Aerospace,* vol. 8, no. 6, p. 163, 2021.

[7] H. Kuhn, A. Seitz, L. Lorenz, A. T. Isikveren and A. Sizmann, "Progress and Perspectives of Electric Air Transport," in *28th Congress of the International Council of the Aeronautical Sciences ICAS*, Brisbane, 2012.

[8] J. Hoelzen, Y. Liu, B. Bensmann, C. Winnefeld, A. Elham, J. Friedrichs and R. Hanke-Rauschenbach, "Conceptual Design of Operation Strategies for Hybrid Electric Aircraft," *Energies,* vol. 11, no. 1, p. 217, 2018.

[9] S. J. Gerssen-Gondelach and A. P. Faaij, "Performance of batteries for electric vehicles on short and longer term".

[10] G. Girishkumar, B. McCloskey, A. C. Luntz, S. Swanson and W. Wilcke, "Lithium−Air Battery: Promise and Challenges," *The Journal of Physical Chemistry Letters,* vol. 1, no. 14, pp. 2193-2203, 2010.

[11] A. Manthiram, Y. Fu and Y.-S. Su, "Challenges and Prospects of Lithium–Sulfur Batteries," *Accounts of Chemical Research,* vol. 46, no. 5, pp. 1125-1134, 2013.

[12] A. W. Schafer, S. R. H. Barrett, K. Doyme, L. M. Dray, A. R. Gnadt, R. Self, A. O'Sullivan, A. P. Synodinos and A. J. Torija, "Technological, economic and environmental prospects of all-electric aircraft," *Nature Energy,* vol. 4, pp. 160-166, 2019.

[13] M. Zhao, B.-Q. Li, X.-Q. Zhang, J.-Q. Huang and Q. Zhang, "A Perspective toward Practical Lithium–Sulfur Batteries," *ACS Central Science,* vol. 6, no. 7, pp. 1095-1104, 2020.

[14] D. E. Calderon, J. E. Cooper, M. Lowensberg, S. A. Neild and E. B. Coetzee, "Sizing High-Aspect-Ratio Wings with a Geometrically Nonlinear Beam Model," *Journal of Aircraft,* vol. 56, no. 4, 2019.

[15] Y. Ma, S. Karpuk and A. Elham, "Conceptual design and comparative study of strut-braced wing and twin-fuselage aircraft configurations with ultra-high aspect ratio wings," *Aerospace Science and Technology,* vol. 121, 2022.

[16] A. D. Gohardani, G. Doulgeris and R. Singh, "Challenges of future aircraft propulsion: A review of distributed propulsion technology and its potential application for the all electric commercial aircraft," *Progress in Aerospace Sciences,* vol. 47, no. 5, pp. 369-391, 2011.

[17] L. Leifsson, A. Ko, W. H. Mason, J. A. Schetz, B. Grossman and R. T. Haftka, "Multidisciplinary design optimization of blended-wing-body transport aircraft," *Aerospace Science and Technology,* vol. 25, no. 1, pp. 16-28, 2013.

[18] C. E. Jones, P. J. Norman, S. J. Galloway, M. J. Armstrong and A. M. Bollman, "Comparison of Candidate Architectures for Future Distributed Propulsion Aircraft," *Transactions on Applied Superconductivity,* vol. 26, no. 6, 2016.

[19] G. Ameyugo, M. Taylor and R. Singh, "Distributed Propulsion Feasibility Studies," *25th International Congress of the Aeronautical Sciences,* 2006.

[20] P. Aref, M. Ghoreyshi, A. Jirasek, M. J. Satchell and K. Bergeron, "Computational Study of Propeller–Wing Aerodynamic Interaction," *Aerospace,* vol. 5, no. 3, p. 79, 2018.

[21] R. A. McDonald, "Advanced Modeling in OpenVSP," in *16th AIAA Aviation Technology, Integration, and Operations Conference*, Washington, D.C., 2016.

[22] EASA, "CS-23 CS-23 Normal, Utility, Aerobatic and Commuter Aeroplanes," European Union Aviation Safety Agency, 2023.

[23] G. P. Chiozzotto, "Initial Weight Estimate of Advanced Transport Aircraft Concepts Considering Aeroelastic Effects," in *55th AIAA Aerospace Sciences Meeting*, Grapevine, TX, 2017.

[24] D. P. Wells, B. L. Horvath and L. A. McCullers, "The Flight Optimization System Weights Estimation Method," 2017.

[25] D. Raymer, Aircraft Design: A Conceptual Approach, 2012.

[26] International Civil Aviation Organization, Annex 14 - Aerodromes - Volume I - Aerodromes Design and Operations, 2022.

[27] W. Johnson, "NDARC NASA Design and Analysis of Rotorcraft," 2017.

[28] T. J. Souders and T. T. Takahasi, "VORLAX 2020: Making a Potential Flow Solver Great Again," in *AIAA Aviation 2021 Forum*, 2021.

[29] M. A. Clarke and R. M. Erhard, "Aerodynamic Optimization of Wing-Mounted Propeller," in *AIAA Aviation 2021 Forum*, Stanford, CA.

[30] "ATR 72-600," 2023. [Online]. Available: https://www.atr-aircraft.com/wp-content/uploads/2022/06/ATR_Fiche72-600-3.pdf. [Accessed 26 April 2023].

[31] "ATR 72-600 Factsheet," June 2015. [Online]. Available: https://www.skybrary.aero/sites/default/files/bookshelf/3696.pdf. [Accessed 26 April 2023].

[32] J. Brousek and T. Zvolsky, "Experimental study of electric vehicle gearbox efficiency," in *10th International Scientific Conference on Aeronautics, Automotive and Railway Engineering and Technologies*, 2018.

[33] S. Stückl, "Methods for the Design and Evaluation of Future Aircraft Concepts Utilizing Electric Propulsion Systems," Technische Universität München, Munich, 2016.

[34] S. Xiang, Y.-q. Liu, G. Tong, W.-p. Zhao, S.-x. Tong and Y.-d. Li, "An improved propeller design method for the electric aircraft," *Aerospace Science and Technology,* vol. 78, pp. 488-493, 2018.

[35] M. K. Bradley and C. K. Droney, "Subsonic Ultra Green Aircraft Research: Phase II – Volume II – Hybrid Electric Design Exploration," Boeing Research and Technology, Huntington Beach, CA, 2015.

[36] S. Gudmunsson, General Aviation Aircraft Design, Butterworth-Heinemann, 2013.

[37] M. D. Patterson, "Conceptual Design of High-Lift Propeller Systems for Small Electric Aircraft," Georgia Institude of Technology, GE, 2016.

[38] R. de Vries, M. Brown and R. Vos, "Preliminary Sizing Method for Hybrid-Electric Distributed-Propulsion Aircraft," *Journal of Aircraft,* vol. 56, no. 6, 2019.

[39] A. K. Kundu, Aircraft Design, Cambridge University Press, 2010.

[40] B. G. Marinus and L. Quodbach, "Data and Design Models for Civil Turbopropeller Aircraft," *JA Aircraft,* vol. 57, no. 6, 2020.

[41] H. Glauert, An aerodynamic theory of the airscrew, HM Stationery Office, 1922.

[42] J. Roskam, Airplane Design: Part 2-Preliminary Configuration Design and Integration of the Propulsion System, DARcorporation, 1985.

[43] D. Howe, Aircraft Conceptual Design Synthesis, London: Professional Engineering Publishing Limited , 2000.

[44] R. T. Taylor and E. J. Ray, "Deep-Stall Aerodynamic Characteristics of T-Tail Aircraft," in *NASA Conference on Aircraft Operating Problems: A Compilation of the Papers Presented*, VA, 1965.

[45] W. Xue, L. Miao, L. Qie, C. Wang, S. Li, J. Wang and J. Li, "Gravimetric and volumetric energy densities of lithium-sulfur batteries," *Current Opinion in Electrochemistry,* vol. 6, no. 1, pp. 92-99, 2017.

[46] J. Z. Bird, "A Review of Electric Aircraft Drivetrain Motor Technology," *IEEE Transactions on Magnetics,* vol. 58, no. 2, 2021.

[47] Y. Ma and A. Elham, "Twin-fuselage configuration for improving fuel efficiency of passenger aircraft," *Aerospace Science and Technology,* vol. 118, 2021.

[48] R. M. Erhard, M. A. Clarke and J. J. Alonso, "A Low-Cost Aero-Propulsive Analysis of Distributed Electric Propulsion Aircraft," in *AIAA Scitech 2021 Forum*, Stanford, CA, 2021.